# Thermal and mechanical properties of the clathrate-II Na<sub>24</sub>Si<sub>136</sub>

Matt Beekman, 1,\* Antti J. Karttunen 0, 2 Winnie Wong-Ng 0, 3 Mingjian Zhang, 4 Yu-Sheng Chen 0, 4 Christian Posadas, 1 Andrew Jarymowycz, 1 E Cruse, 1 Wanyue Peng, 5 Alexandra Zevalkink, 5 James A. Kaduk 0, 6, 7 and George S. Nolas 8, † 1 Department of Physics, California Polytechnic State University, San Luis Obispo, California 93402 USA 2 Department of Chemistry and Materials Science, Aalto University, FI-00076 Aalto, Finland 3 Materials Measurement Science Division, National Institute of Standards and Technology (NIST), Gaithersburg, Maryland 20899, USA 4 ChemMatCARS, University of Chicago, Lemont, Illinois 60439, USA 5 Department of Chemical Engineering and Materials Science, Michigan State University, East Lansing, Michigan 48824 USA 6 Department of Chemistry, Illinois Institute of Technology, Chicago, Illinois 60616, USA 7 Department of Physics, North Central College, Naperville, Illinois 60540, USA

<sup>8</sup>Department of Physics, University of South Florida, Tampa, Florida 33620, USA

(Received 17 March 2022; revised 27 May 2022; accepted 3 June 2022; published 30 June 2022)

Thermal expansion, lattice dynamics, heat capacity, compressibility, and pressure stability of the intermetallic clathrate Na<sub>24</sub>Si<sub>136</sub> have been investigated by a combination of first-principles calculations and experimentation. Direct comparison of the properties of Na<sub>24</sub>Si<sub>136</sub> with those of the low-density elemental modification Si<sub>136</sub> provide insight into the effects of filling the silicon clathrate framework cages with Na on these properties. Calculations of the phonon dispersion only yield sensible results if the Na atoms in the large cages of the structure are displaced from the cage centers, but the exact nature of off-centering is difficult to elucidate conclusively. Pronounced peaks in the calculated phonon density of states for Na<sub>24</sub>Si<sub>136</sub>, absent for Si<sub>136</sub>, reflect the presence of low-energy vibrational modes associated with the guest atoms, in agreement with prior inelastic neutronscattering experiments and reflected in marked temperature dependence of the guest atom atomic displacement parameters determined by single-crystal x-ray diffraction. The bulk modulus is only weakly influenced by filling the Si framework cages with Na, whereas the phase stability under pressure is significantly enhanced. The roomtemperature linear coefficient of thermal expansion (CTE) is nearly a factor of 3 greater for Na<sub>24</sub>Si<sub>136</sub> compared to Si<sub>136</sub>. Negative thermal expansion (NTE), observed in Si<sub>136</sub> below 100 K, is noticeably absent in Na<sub>24</sub>Si<sub>136</sub>. In contrast to Si<sub>136</sub>, the thermal expansion behavior in Na<sub>24</sub>Si<sub>136</sub> is relatively well described by the conventional Grüneisen-Debye model in the temperature range of 10–700 K. First-principles calculations in the quasiharmonic approximation correctly predict an increase in high-temperature CTE with Na loading, although the increase is less than observed in experiment. The calculations also fail to capture the absence of NTE in Na<sub>24</sub>Si<sub>136</sub>, perhaps due to anharmonic effects and/or inadequateness of the ordered structural model.

DOI: 10.1103/PhysRevB.105.214114

# I. INTRODUCTION

Intermetallic clathrates are crystalline compounds characterized by structures with expanded covalently bonded frameworks that can encapsulate a variety of different "guest" atoms [1]. Guest-free variants, such as Si<sub>136</sub> [2] and Ge<sub>136</sub> [3] constitute novel low-density crystalline elemental modifications (allotropes) that have interesting optical and thermal properties [4]. In addition, Si<sub>136</sub> was found to be surprisingly stable with respect to temperature [5] and pressure [6,7]. On the other hand, the clathrates with guest atoms occupying the framework cages have attracted much attention due to their potential for use as thermoelectric materials [1,8,9] as well as fundamentally interesting behavior, such as glasslike thermal conductivity in crystalline solids [10,11], the underlying mechanisms for which have been the topic of much inquiry

[1,10–12]. The superconducting, magnetic, and mechanical properties of clathrates have also received considerable attention as has their fundamental crystal chemistry [1].

Significant theoretical and experimental work over the past many years has shown that the guest atoms, or, more precisely, the guest-framework interactions, play an important role in many of the interesting properties of intermetallic clathrates [1,9–12]. The low and sometimes glasslike thermal conductivity is in large part attributed to low-energy guest atom vibrations that simultaneously enhance phonon scattering and reduce phonon velocities and Debye temperatures through an avoided crossing in the phonon dispersion and overall lowering of phonon frequencies [1,9-14]. The type of guest can also be manipulated to influence the electronic structure and improve the thermoelectric performance by increasing the density of states near the Fermi level [15]. It would be instructive if one could vary the guest content in a particular clathrate to directly observe the effect of guest content on the various physical properties. Whereas this can be readily performed using first-principles calculations [13], it is unfortunately

<sup>\*</sup>mbeekman@calpoly.edu

<sup>†</sup>gnolas@usf.edu

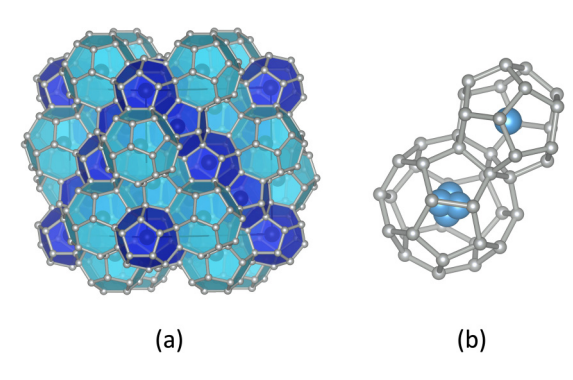


FIG. 1. (a) Crystal structure of  $Na_{24}Si_{136}$ . Silicon framework atoms are shown as smaller light gray spheres, whereas the Na guests are shown as dark spheres. The  $Si_{20}$  and  $Si_{28}$  polyhedra are shaded in blue and teal, respectively. In this representation, all guest atoms are centered in the framework polyhedra. (b) Fragment of the crystal structure of  $Na_{24}Si_{136}$  showing the  $Si_{20}$  and  $Si_{28}$  polyhedra. The off-center position for the Na guest in the  $Si_{28}$  cage (32e site, four equivalent positions per  $Si_{28}$  cage) used in the structure refinements is depicted.

difficult to pursue experimentally, as the guest content in nearly all known intermetallic clathrates is fixed at full or nearly full occupation with very few exceptions [1].

One such exception is the Na<sub>x</sub>Si<sub>136</sub> (0 <  $x \le 24$ ) system with the clathrate-II structure (see Fig. 1) [16], which is also perhaps the most studied of all the known intermetallic clathrate compositions. Remarkably, despite the attention they have received and the fact that the Na<sub>x</sub>Si<sub>136</sub> clathrates were the first intermetallic clathrates to be discovered more than half a century ago [17,18], a full understanding of many aspects of the properties and even the structure and stability of these interesting materials have yet to be unequivocally established. Chemically interesting in the sense that the fully filled end member (x = 24) is a stoichiometric compound and a good metal [19], whereas the empty end member  $(x \sim 0)$  corresponds to a metastable low-density crystalline modification of silicon that is a wide band-gap semiconductor [2], the ability to vary the guest content continuously in these materials provides an opportunity to study the effect of the guest atoms on electrical and thermal properties of intermetallic clathrates [20–22]. Previous theoretical and experimental work has elucidated how the open-framework structure in the Si<sub>136</sub> modification affects the thermal, electronic, and mechanical properties of this low-density form of this technologically important chemical element. Noteworthy features of Si<sub>136</sub> include a much-lowered lattice thermal conductivity [23,24] and expanded indirect band gap [2,25] relative to  $\alpha$ -Si and relatively low compressibility and unexpected stability with respect to pressure [6,7]. Filling the cages with Na produces interesting and still not completely understood behavior, including a pronounced increase in the thermal expansion coefficient near room temperature [22] and a metal-insulator transition near  $x \approx 8$  [20] that is correlated with a nonmonotonic structural response to filling [26]. In the present paper, we have used a combination of first-principles calculations and experiment to investigate thermal expansion, lattice dynamics, heat capacity, compressibility, and pressure stability of clathrate-II Na<sub>24</sub>Si<sub>136</sub>. Direct comparison with

Si<sub>136</sub> allows inferences to be made about the effect of filling the Si<sub>136</sub> cages with Na on these properties, providing insights into the effects of guest content on lattice dynamics and mechanical properties.

## II. COMPUTATIONAL DETAILS

We used density functional theory (DFT) with the Perdew-Burke-Ernzerhof (PBE) exchange-correlation functional and Garrity-Bennett-Rabe-Vanderbilt ultrasoft pseudopotentials to study the phonon properties of Si<sub>136</sub> and Na<sub>24</sub>Si<sub>136</sub> [27,28]. DFT calculations were carried out with the QUANTUM ESPRESSO (QE) package (version 6.4) [29]. The PHONOPY code was used to study the phonon properties with the harmonic and quasiharmonic approximations [29–31]. In all QE calculations, electron kinetic-energy cutoffs of 40 and 200 Ry were applied for wave functions and charge densities, respectively. A  $3 \times 3 \times 3$  Monkhorst-Pack type k mesh was used for sampling the reciprocal space. A 0.005-Ry Gaussian smearing was used for the Brillouin-zone integration in the case of Na<sub>24</sub>Si<sub>136</sub>. The studied structures were fully optimized within their respective space-group symmetries. Tight convergence criteria were applied for the structural optimizations (10<sup>-6</sup> and 10<sup>-5</sup> a.u. for energies and forces, respectively). A very tight self-consistent field convergence criterion (10<sup>-10</sup> a.u.) was used in all calculations. The optimized structure of Na<sub>24</sub>Si<sub>136</sub> that was used for calculation of the phonon dispersion is provided in the Supplemental Material [32].

In the finite-difference phonon supercell calculations with PHONOPY,  $2 \times 2 \times 2$  phonon supercells with default displacements of 0.02 bohr were applied. A  $2 \times 2 \times 2$  Monkhorst-Pack type k mesh was used for sampling the reciprocal space in the supercell calculations. Phonon density of states were evaluated using tetrahedron integration and phonon q meshes of  $30 \times 30 \times 30$  and  $24 \times 24 \times 24$  for  $\mathrm{Si}_{136}$  and  $\mathrm{Na}_{24}\mathrm{Si}_{136}$ , respectively. Quasiharmonic phonon properties were obtained by calculating the thermal properties at five different volumes  $(-1\%, -0.5\%, 0\%, +0.5\%, +1.0\%; 2 \times 2 \times 2$  supercell) and fitting the thermal properties with PHONOPY-QHA. Thermal properties were evaluated using a q mesh of  $40 \times 40 \times 40$ . The electronic contribution to heat-capacity  $C_v$  was evaluated with the THERMOPW code, using an electronic k mesh of  $12 \times 12 \times 12$  [33].

The bulk moduli at 0 K were evaluated using the CRYS-TAL17 program package and hybrid PBE0 density functional method [34,35]. Gaussian-type orbital bases were used (triple- $\zeta$ -valence + polarization for Si, split-valence + polarization for Na) [36-38]. The structures were optimized with the default optimization convergence criteria in CRYSTAL17, and the lowest-energy structures were confirmed to be true local minima by means of harmonic frequency calculations. Tightened tolerance factors of 8, 8, 8, 8, and 16 were used for the evaluation of the Coulomb and exchange integrals. Similar k meshes were used for reciprocal space integration as in the QE calculations. For Na<sub>24</sub>Si<sub>136</sub>, a denser  $6 \times 6 \times 6 \times 6$  mesh was used for the evaluation of the Fermi energy, and a Fermi smearing of 0.002 a.u. was applied. The energy-volume data were fitted to Birch-Murnaghan equation of state to obtain the bulk moduli (six different volumes, 92%-108% of the original cell volume) [39].

#### III. EXPERIMENTAL DETAILS

## A. Sample preparation

Single-crystal Na<sub>24</sub>Si<sub>136</sub> specimens were prepared according to the procedure described previously [40]. Phase purity and composition were confirmed by laboratory powder x-ray diffraction (XRD) and energy dispersive spectroscopy, respectively, with no impurity phases detected.

#### B. High pressure power x-ray diffraction

In situ high-pressure powder synchrotron XRD experiments were conducted at room temperature at the Advanced Photon Source (APS) at Argonne National Laboratory, beamline 13-BM-C (GSECARS). The as-synthesized crystals grown by the approach referenced above were ground into powder with grain sizes smaller than 1  $\mu$ m, which were then pressed into flakes before loading into a diamond-anvil cell. The benefit of using flakes is for the convenience of sample loading as well as an increased amount of material per unit area. Ruby was placed next to the sample to calibrate the pressure readings. Diamond anvils with culet sizes of 300 µm were used with rhenium metal gaskets from H-Cross preindented to thickness of approximately 45  $\mu$ m. The preindented gaskets were drilled in the center to form a hole about half of the corresponding anvil size using an electrical discharge machine at Michigan State University. Neon was loaded as the hydrostatic pressure medium using the COM-PRES/GSECARS gas-loading system for all samples. During the measurements, pressures were changed remotely via a gasmembrane setup. The values of the pressure were read in situ via the ruby fluorescence system before and after each data collection [41]. The distance and orientation of the detector were calibrated using a CeO<sub>2</sub> standard. The beam size was 12  $\mu$ m (horizontal) × 18  $\mu$ m (vertical) full width at half maximum. The detector was an online Pilatus 1-M image plate. Diffraction data were collected using the x-ray wavelength of 0.4133 Å at pressures from 0.5 to 18 GPa with an exposure time of 240 s for each scan. The DIOPTAS program [42] was used for raw data processing. The cubic lattice parameter of Na<sub>24</sub>Si<sub>136</sub> at each pressure was subsequently determined from least-squares refinement using the extracted peak positions, which were obtained by fitting the peaks using the FITYK software [43].

## C. Temperature-dependent single-crystal x-ray diffraction

A crystal of size  $20 \times 30 \times 35~\mu\text{m}^3$  was mounted with paratone oil on the tip of a glass fiber. Single-crystal x-ray diffraction measurements were carried out at NSF's ChemMatCARS, Sector 15 of the APS, Argonne National Laboratory. Data were collected using a Huber three-circle diffractometer equipped with a Pilatus  $3 \times 2$ -M detector and the sample temperature was controlled using an Oxford Cryojet. The experiments were performed using liquid N<sub>2</sub> (from 290 K down to 102 K) or liquid helium (from 60 to 10 K).

<sup>1</sup>Certain trade names and company products are mentioned in the text or identified in illustrations in order to adequately specify the experimental procedures and equipment used. In no case does such

During data collection, the  $\omega$  angle was set to  $-180^\circ$ ,  $\kappa$  angle was set to  $0^\circ$  and  $30^\circ$  with the  $\phi$  angle scanned over the range of  $360^\circ$  using the shutterless mode of the detector with the x-ray wavelength  $\lambda=0.41328\,\text{Å}$ . Data integration was performed with Bruker APEX 3 suite software [44]. Data reduction was conducted with the SAINT V.8.38 and SADABS V.2016 programs included in the APEX suite. The crystal structure at each temperature was solved by direct methods and refined by the full-matrix least-squares on  $F^2$  [45,46]. Table S2 to S3 in the Supplemental Material [32] give the refinement residuals, crystallographic data, and anisotropic displacement parameters  $(U_{ij})$ .

#### IV. RESULTS AND DISCUSSION

# A. Phonon dispersion

We first discuss the effects of filling the Si framework cages with Na guests on the phonon dispersion. The Na<sub>24</sub>Si<sub>136</sub> clathrate-II structure [16,40] can be described as a fourbonded silicon framework formed by face sharing of Si<sub>20</sub> and Si<sub>28</sub> polyhedral cages in a 2:1 ratio in which the Na atoms reside (see Fig. 1). Initially, phonon dispersion curves were calculated assuming the equilibrium positions for both Na guest atoms to be located at the centers of the Si<sub>20</sub> and Si<sub>28</sub> cages, respectively. However, this resulted in the appearance of modes with imaginary frequencies in the phonon dispersion, indicative of a dynamical instability associated with the guest atoms in Na<sub>24</sub>Si<sub>136</sub>. Prior structure refinements using single crystal [20,40,47] and powder diffraction [26] have shown that, when assumed to occupy the crystallographic site at the cage center, the atomic displacement parameter for  $Na@Si_{28}$  (the "@" symbol designates the guest in question) becomes unreasonable large. Various models have been used to describe the crystal structure of Na<sub>24</sub>Si<sub>136</sub>, although the available diffraction studies to date have not yet been able to conclusively discern which structural model best reflects the true structure, i.e., different models for the Na@Si<sub>28</sub> guest atom typically fit the data more or less equally well [20,26,40,47,48]. Extended x-ray absorption fine-structure analysis [49,50] suggested a dimerization of Na guests in adjacent cages such that the Na@Si<sub>28</sub> guests shift off-center toward each other along the direction perpendicular to the shared hexagonal face of adjacent Si<sub>28</sub> cages. A related model has been applied in structure refinements using powder-diffraction data for  $Na_xSi_{136}$  (x < 24) [26] where the Na@Si<sub>28</sub> guest atoms randomly occupy one of four equivalent positions in the large cage that are shifted off-center toward the hexagonal face of the Si<sub>28</sub> cage with the extent of the shift becoming more pronounced as the Na content decreases [26,51,52]. We note that diffraction data cannot differentiate between ordered dimerization vs random dimerization vs random off-centering (disorder). With all this in mind, to make first-principles calculations tractable we performed calculation of the phonon dispersion using an ordered model with space-group  $R\bar{3}m$  in which the guest atoms inside adjacent

identification imply recommendation or endorsement by the National Institute of Standards and Technology.

Si<sub>28</sub> cages are shifted approximately 0.35 Å off-center toward their common hexagonal face, similar to the Na dimer model. Interestingly, this displacement, obtained through full geometry optimization (Na@Si20 still on-center; see the Supplemental Material [32]), is very similar to the Na@Si<sub>28</sub> displacement experimentally observed in diffraction experiments [26]. Employing this structure model resulted in only real phonon modes, supporting the notion that the Na guests in the Si<sub>28</sub> cage are indeed likely shifted off-center in the large cage. To further explore the nature of the off-centering, we also performed a potential energy scan by intentionally displacing the Na@Si<sub>28</sub> guest toward and away from the hexagonal face and found two shallow minima each about 0.35 Å from the cage center (fractional coordinates of 0.390 and 0.360, respectively, where the on-center is 0.375 in the  $R\bar{3}m$  model), suggesting the existence of multiple off-center equilibrium positions. In addition, the total energy decreases by less than 0.3 kJ/mol due to the off-centering, reflecting the fact that the potential-energy landscape for this guest atom is relatively flat throughout a significant fraction of the volume of the cage. The actual equilibrium position of the Na@Si<sub>28</sub> guest may, therefore, be strongly disordered from cage to cage, or perhaps even within a single cage dynamically via hopping or tunneling though the relatively low potential barrier. We discuss some of these aspects of the structure more in Sec. II C below.

The calculated phonon dispersion curves and phonon density of states for Si<sub>136</sub> and Na<sub>24</sub>Si<sub>136</sub> (Na@Si<sub>28</sub> off-center model) are shown in Fig. 2, respectively. The phonon dispersion relations obtained for Si<sub>136</sub> in the present paper are in good agreement with previous computational studies on the same material using DFT-local-density approximation and DFT-generalized gradient approximation methods [24,53]. The mostly likely reason for slight differences in the density of states shown in Fig. 2 as compared to Ref. [53] is the use of tetrahedron integration (used here) vs Gaussian smearing during the integration of density of states (used in Ref. [53]). Whereas there are some general features in the phonon dispersion of Si<sub>136</sub> and Na<sub>24</sub>Si<sub>136</sub> that are similar, there are also several conspicuous differences, in qualitative agreement with previous inelastic neutron-scattering (INS) experiments on  $Na_xSi_{136}$  (x = 3,23) [47]. Several lower-energy optical modes appear in two separate regions: (i) in the range of 100–160 cm<sup>-1</sup> corresponding to the optic mode region of the Si<sub>136</sub> framework, and (ii) relatively dispersionless "rattler" modes in the range of the acoustic modes for the "host" Si<sub>136</sub> structure, resulting in an avoided crossing or "anticrossing' of the host acoustic and low-energy guest optical modes [54]. This avoid-crossing effect has been theoretically and experimentally observed in several other intermetallic clathrate compositions [1,9,11-13,16]. As shown in Fig. 2, projection of the density of states onto the Na@Si<sub>20</sub> guest, Na@Si<sub>28</sub> guest, and Si framework atoms reveals that the lowest-energy optical modes can be attributed to Na@Si28, whereas a significant fraction of the modes in the range of 100–160 cm<sup>-1</sup> involve the Na guests in the smaller Si<sub>20</sub> cages. The energies of the Na@Si<sub>20</sub> modes are in relatively good agreement with those inferred by previous powder INS from Na<sub>23</sub>Si<sub>136</sub>, as well as the temperature dependence of atomic displacement parameters [47] and heat-capacity measurements [19]

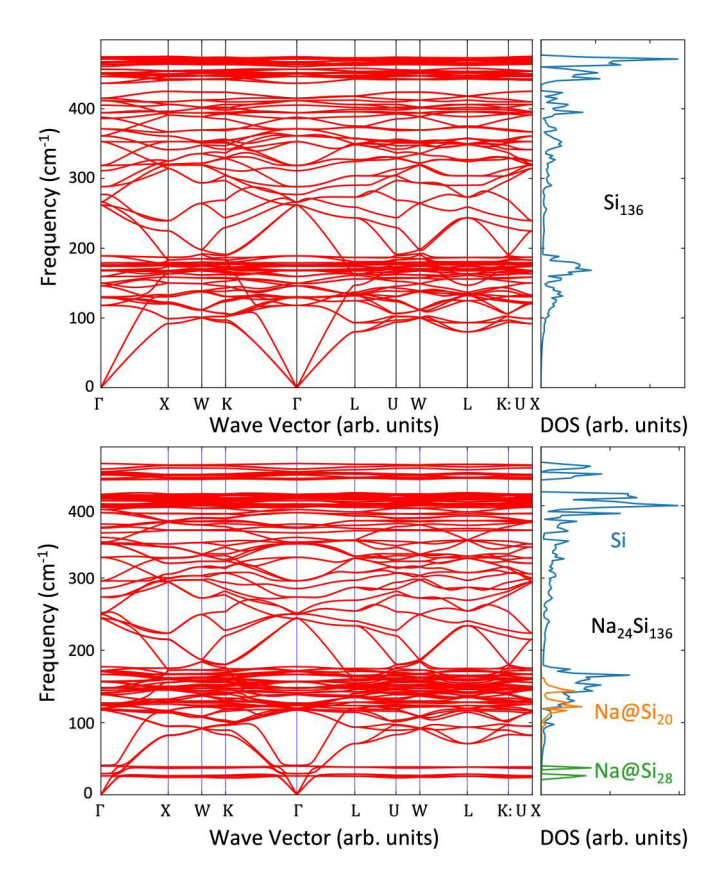


FIG. 2. Calculated phonon dispersion (left) and vibrational density of states (right) for  $Si_{136}$  (top) and  $Na_{24}Si_{136}$  (bottom). The projected density of states in (the lower panel) shows the contributions of the  $Na@Si_{28}$  guests (green),  $Na@Si_{20}$  guests (orange), and Si framework atoms (blue) to the total vibrational density of states. The primitive cells of  $Si_{136}$  ( $Fd\bar{3}m$ ) and ordered  $Na_{24}Si_{136}$  model ( $R\bar{3}m$ ) are closely related, thus, although the structure models for the clathrate are not strictly the same, wave-vector coordinates, and labels for  $Fd\bar{3}m$  ( $Si_{136}$ ) were used in both cases to facilitate comparisons between the two crystal structures; see Ref. [56].

for Na<sub>24</sub>Si<sub>136</sub>. In contrast, the calculated Na@Si<sub>28</sub> modes are very flat and appear separated into two narrow energy ranges that are somewhat lower in energy than has been previously inferred by experiment [19,47]. The higher-energy Na@Si<sub>28</sub> modes in Fig. 2 are due to Na rattling parallel to the offcentering direction (in which the Na atom moves closer to the Si atoms in this direction, experiencing a larger restoring force; symmetry  $A_{1g} + A_{2u}$ ), whereas the lower-energy Na@Si<sub>28</sub> modes are due to Na rattling perpendicular to the off-center displacement (symmetry  $E_{\rm u} + E_{\rm g}$ ). The relatively low dispersion for these modes is due to the fact that they are dominated by the Na@Si28 vibrations and the Na-Si interaction for this guest is significantly weaker than the Si-Si interaction of the framework. The fact that the predicted energies of the Na@Si<sub>28</sub> modes are somewhat lower than observed in experiment, and that experiments have not resolved two such branches, could be an indication that the position and dynamics the Na@Si<sub>28</sub> guest atoms are not completely captured by the simple ordered structure model, and/or anharmonicity is important. Moreover, both inter- and intracage disorders in the off-centering are likely present, making the guest atom

dynamics and their effects on the dispersion more complex and difficult to model. Xue and Myles provided an indication from first-principles calculation that the effective potential that Na@Si<sub>28</sub> in Na<sub>24</sub>Si<sub>136</sub> experiences is broad and relatively flat with no clear off-center minimum (in general agreement with our results discussed above) and concluded the anharmonic rattling results in a strongly temperature-dependent rattling frequency, increasing by more than a factor of 3 from 0 K to room temperature [52]. We, therefore, conclude that the anharmonic Na@Si<sub>28</sub> rattling may not be well described by the harmonic approximation applied here. It is also possible that the DFT-PBE method used here underestimates the strength of the Na-Si interactions and, thus, the energies of the Na@Si<sub>28</sub> modes.

Regarding the behavior of the silicon vibrational modes, upon introduction of Na into the Si<sub>20</sub> and Si<sub>28</sub> cages, the optical modes associated with the Si framework generally shift to lower energies. This behavior for the optical modes has also been observed in previous INS studies on Na<sub>x</sub>Si<sub>136</sub> [47,55]. We note that the Na guests do not contribute appreciably to the vibrational density of states for frequencies above approximately 160 cm<sup>-1</sup> [see Fig. 2]. The frequency lowering of the silicon framework optical modes can be attributed, at least, in part to the expansion of the lattice due to Na loading and corresponding weakening of the Si-Si framework bonding.

## B. High pressure x-ray diffraction

Prior work has shown the low density expanded framework elemental modification Si<sub>136</sub> to be remarkably stable with respect to pressure [6,7]. Indeed, the Si<sub>136</sub> clathrate framework remains intact to pressures greater than 8 GPa, above which it directly transforms to the  $\beta$ -Si ( $\beta$ -Sn) structure. This transition pressure, which is not too much smaller than that for the  $\alpha$ -Si to  $\beta$ -Si transition, is substantially higher than would be expected from simple thermodynamic arguments. Rather, the high transition pressure has been attributed to the strong Si-Si bonds and the lack of a low-energy pathway for atomic rearrangement [7]. It was also found that the clathrate-II Si<sub>136</sub> modification with a bulk modulus of  $B_0 \approx 90 \, \text{GPa}$ is only slightly more compressible than  $\alpha$ -Si ( $B_0 \approx 97$  GPa) [6,7]. Thus, despite its lower density open framework structure, Si<sub>136</sub> can be classified as a relatively low compressibility material. Theoretical calculations have provided some insight into the effects of incorporating guest atoms in the framework cages on the pressure stability and elastic properties, but few experimental studies of the direct effect of guest atoms on the pressure stability have been carried out [57].

Room-temperature powder XRD data were collected as a function of pressure from a specimen of Na<sub>24</sub>Si<sub>136</sub>. To the highest pressure we were able to investigate, which was 18 GPa in our experiment, no structural transition in Na<sub>24</sub>Si<sub>136</sub> was observed—all diffraction peaks could be indexed to the clathrate-II structure. Thus, the filled Na<sub>24</sub>Si<sub>136</sub> clathrate is substantially more stable with respect to pressure than Si<sub>136</sub>. Interestingly, clathrate-II Na<sub>24</sub>Si<sub>136</sub> also appears to be significantly more stable with respect to pressure than clathrate-I Na<sub>8</sub>Si<sub>46</sub> (which experiences a first-order structural transition near 13 GPa to the high-pressure hexagonal phase of elemental silicon [6]), despite the very similar composition (Na:Si

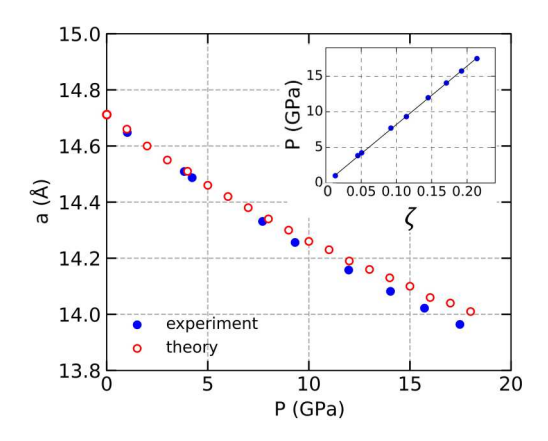


FIG. 3. Measured (closed circles, room temperature) and theoretically calculated (open circles, 0 K) cubic lattice parameter a as a function of pressure for Na<sub>24</sub>Si<sub>136</sub>. The inset: Plot of pressure vs  $\zeta = \frac{3}{2}[(V_0/V)^{7/3} - (V_0/V)^{5/3}]$ , where V and  $V_0$  are the experimental unit-cell volumes at pressure P and ambient pressure, respectively.

ratio), atomic density, and bonding arrangements for these two Na-Si clathrate compounds. The fully filled Na<sub>24</sub>Si<sub>136</sub> clathrate also has a significantly greater pressure stability than partially filled Na<sub>x</sub>Si<sub>136</sub> (0 < x < 24), for which phase transitions to the  $\beta$ -Sn structure were reported to occur between 8 and 12 GPa [58].

The experimental and theoretically predicted cubic lattice parameter of  $Na_{24}Si_{136}$  is plotted as a function of pressure in Fig. 3. The experimental lattice parameter at ambient pressure,  $a = 14.712 \,\text{Å}$  is in very good agreement with prior work [26,40,48]. We note that the experimental and theoretically predicted lattice parameters in Fig. 3 are at ambient temperature and 0 K, respectively, thus, the quantitative agreement should be considered fortuitous. To directly compare to the reported experimental bulk modulus of  $Na_{24}Si_{36}$  to that of  $Si_{36}$ , we first linearized the Birch-Murnagham equation of state [59,60],

$$P(V) = \frac{3B_0}{2} \left[ \left( \frac{V_0}{V} \right)^{7/3} - \left( \frac{V_0}{V} \right)^{5/3} \right] \times \left\{ 1 + \frac{3}{4} (B_0' - 4) \left[ \left( \frac{V_0}{V} \right)^{2/3} - 1 \right] \right\}, \tag{1}$$

where V and  $V_0$  are the unit-cell volumes at pressure P and ambient pressure, respectively, and fit our experimental data assuming the first pressure derivative  $B'_0 = 4.00$  (inset to Fig. 3). This analysis yielded a value of  $B_0 = 82(1)$  GPa for the bulk modulus of  $Na_{24}Si_{136}$ , which is only a few percent smaller than the value of  $B_0 = 87(3)$  GPa determined previously for Si<sub>136</sub> using the same analysis approach [27]. A more sophisticated analysis using the Eulerian finite-strain method [59,60] yielded a value of  $B_0 = 85 \,\text{GPa}$  and  $B_0' = 4.0$  for Na<sub>24</sub>Si<sub>136</sub>, compared to 90 GPa and 5.2(8) for Si<sub>136</sub> obtained by the same analysis [7]. Relative to  $Si_{136}$ , the bulk modulus of Na<sub>24</sub>Si<sub>136</sub> is, therefore, only about 6% lower, indicating the incorporation of Na into the Si framework cages tends to make the material slightly more compressible. The bulk modulus of metallic Na<sub>24</sub>Si<sub>136</sub> is still relatively high, only  $\sim$ 15%–20% smaller than elemental  $\alpha$ -Si. Our first-principles calculation of the bulk moduli for Si<sub>136</sub> and Na<sub>24</sub>Si<sub>136</sub> at 0 K

TABLE I. Experimental and theoretical bulk moduli B and first pressure derivative B' for  $Si_{136}$  and  $Na_{24}Si_{136}$  (DFT-PBE0/TZVP level of theory).

	Experiment $(T = 294 \text{ K})$		Theory $(T = 0 \text{ K})$	
	B (GPa)	B'	B (GPa)	B'
Si <sub>136</sub>	90ª	5.2ª	85	4.1
$Na_{24}Si_{136} \\$	85	4.0	86	4.7

<sup>&</sup>lt;sup>a</sup>Reference [7].

(using the off-center structural model for the latter, described in Sec. IV A above) and fitting the calculated energy vs volume to the Birch-Murnagham equation of state yielded nearly identical values for B<sub>0</sub> for Si<sub>136</sub> and Na<sub>24</sub>Si<sub>136</sub> (see Table I), further supporting the conclusion that the bulk modulus is only weakly affected by the incorporation of the Na guest into the Si framework cages. The increase in unit-cell size and weakened framework bonding induced by filling the Si<sub>20</sub> and Si<sub>28</sub> cages (population of antibonding states) might be expected to increase the compressibility of the framework, and these aspects perhaps offset the chemical pressure effects associated with filling the open space by occupation of the cages with Na. A recent study of the effect of filler atoms on the bulk modulus of  $M_{0.5}Co_4Sb_{12}$  (M = K, Sr, La, Ce, and Yb) filled skutterudites showed that, whereas all filler atoms cause a lattice expansion relative to unfilled Co<sub>4</sub>Sb<sub>12</sub> for some compositions filling the voids increases  $B_0$ , whereas for other compositions  $B_0$  is little affected or even decreases [61]. Thus, simple arguments based on the internal pressure generated by the guest atoms were not sufficient to explain the observed behavior, and other effects, such as charge transfer are important.

To further explore how the structure evolves under pressure, we performed full geometry optimizations (DFT-PBE0/TZVP level of theory) for Si<sub>136</sub> and Na<sub>24</sub>Si<sub>136</sub> at applied pressures of 0, 5, 10, and 15 GPa. We find that both the silicon framework atom positions as well the Na@Si28 position show systematic changes as pressure is increased. First, the off-center displacement for Na@Si28 was found to quickly drop to zero (Fig. S2 of the Supplemental Material [32]), i.e., the application of pressure has a strong effect of decreasing the off-centering of the Na guest in the larger cage. Similar results have been observed in experimental work on some type-I clathrates [62,63]. Second, we also find that the framework does not compress uniformly. Specifically, the absolute and percent change in the silicon framework atom to cage center distances for the smaller Si<sub>20</sub> cage generally show smaller decreases than the absolute and percent change for the framework to cage center distances for the larger Si<sub>28</sub> cage. Interestingly, this occurs for both Si<sub>136</sub> and Na<sub>24</sub>Si<sub>136</sub>, suggesting the framework geometry is the determining factor for this behavior as opposed to the guest-framework interaction.

## C. Heat capacity

Figure 4 shows the heat capacity of Na<sub>24</sub>Si<sub>136</sub> calculated from first principles using the phonon dispersion in Fig. 2, compared to the experimental data reported previously in

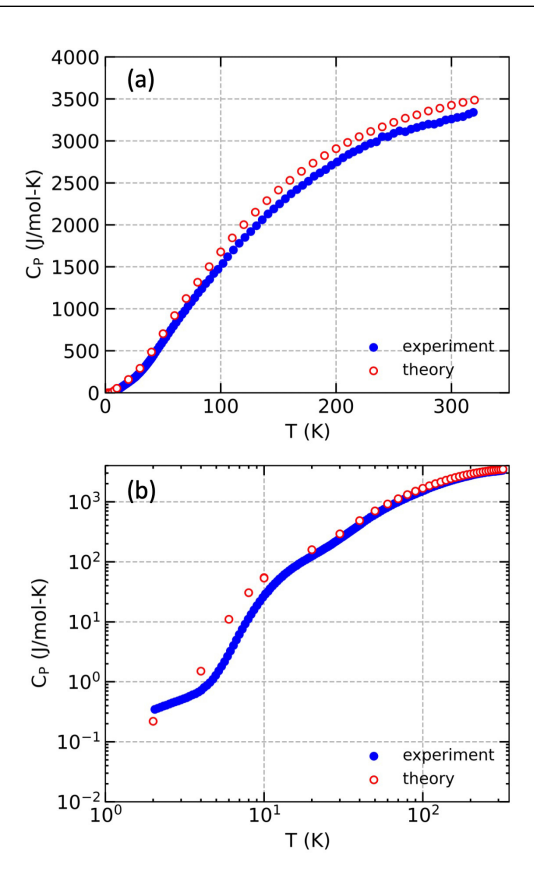


FIG. 4. Calculated and experimental (Ref. [19]) molar heat capacity for  $Na_{24}Si_{136}$  plotted on (a) linear and (b) log-log scales. Estimated uncertainty in the experimental heat-capacity values is  $\leqslant 5\%$ .

Ref. [19]. A theoretically predicted electronic contribution to the heat capacity of Na<sub>24</sub>Si<sub>136</sub> at low temperature has been included in the calculated values plotted in Fig. 4 [33]. Previous experimental and theoretical work have shown that the heat capacity of Si<sub>136</sub> at low T exhibits behavior typical of most crystalline solids and is well described by the Debye model, reflected in a  $T^3$ -temperature dependence at low T [23]. In contrast,  $C_P(T)$  at low T for Na<sub>24</sub>Si<sub>136</sub> shows a vibrational contribution that is not explained by a linear phonon dispersion alone but could be well fit using a sum of electronic, Debye, and two Einstein oscillator contributions to the heat capacity, the latter modeling the Na guest vibration contributions to the heat capacity in molar fractions that agree well with the Na@Si<sub>28</sub>:Na@Si<sub>20</sub>:Si ratio of 8:16:136 [19]. We reiterate that, according to the calculated phonon dispersion in Fig. 2, the modes associated with the Na@Si<sub>20</sub> guest vibrations, whereas relatively flat, have a range of frequencies so that the single Einstein frequency is likely an oversimplification. The calculated heat capacity shown in Fig. 4 is in relatively good qualitative agreement with the experimental data, further supporting the previous interpretation of the low-temperature behavior of  $C_P$  in terms of the low-energy Na vibrations. We note, however, that the calculated  $C_P$  is noticeably larger than the experimental  $C_P$  over the entire temperature range, which could be due to an underprediction of the phonon frequencies for Na<sub>24</sub>Si<sub>136</sub>. This again could be an indication that the model we have used for computation

of the dynamical properties is insufficient to fully capture the physics of the guest dynamics and guest-framework interaction, in particular, the anharmonic nature of the lattice dynamics.

# D. Temperature-dependent single-crystal x-ray diffraction

Guided by the above observations and prior work [26,47,49,50], single-crystal structure refinements were carried out assuming a model in which the Na@Si<sub>28</sub> guest atom is displaced from the Si<sub>28</sub> cage center toward the hexagonal face of the cage as described above. Since the diffraction data cannot discern between ordered vs disordered off-centering, we employed a model in which the Na@Si<sub>28</sub> guest randomly occupies the 32e site (space-group  $Fd\bar{3}m$ ) [26]; detailed crystallographic data and refinement results can be found in the Supplemental Material [32].

Although the refined atomic displacement parameters for the Na@Si<sub>28</sub> guest are significantly smaller for the off-center model in comparison to the on-center model, in agreement with prior work [26,47], they remain exceptionally large even at lower temperatures where the thermal motion contribution to the ADP would be expected to freeze out. Curiously, the refined displacement of the Na@Si<sub>28</sub> guest from the cage center decreases from  $\approx 0.3 \,\text{Å}$  at 290 K to nearly zero at 60 K. In other words, the structure refinements suggest that the Na@Si<sub>28</sub> guest moves further away from the center of the Si<sub>28</sub> cage as the temperature is increased. A similar behavior was observed for the Ba guest in clathrate-I Ba<sub>8</sub>Ga<sub>16</sub>Ge, although in that case the off-centering displacement asymptotically approached a constant nonzero value as temperature was decreased [64]. This behavior could reflect an actual shift in the equilibrium position of the Na@Si<sub>28</sub> guest, or the increased probability of finding the guest atom farther from the center of the cage as temperature increases and the amplitude of motion in the anharmonic potential well increases. Since the atomic displacement parameters are strongly correlated with the off-center displacement, it is difficult to disentangle these effects. These results provide further indication that the nature of the Na guest in the Si<sub>28</sub> cage is complex and not completely captured by a simple off-center (split-site) model. We note that previous x-ray powder-diffraction refinements for  $Na_xSi_{136}$  (0 < x < 24) have suggested that the off-centering becomes more pronounced as x decreases, perhaps due to the presence of empty adjacent Si<sub>28</sub> cages [26,51]. In their first-principles study of  $Na_xSi_{136}$  (x = 4, 8, 12, 16, and 24), Xue and Myles estimated the effective potential experienced by Na@Si<sub>28</sub> and found clear off-center potential minima for Na<sub>4</sub>Si<sub>136</sub>, whereas the potential well was significantly flatter (without clear off-center minima) in the case of Na<sub>24</sub>Si<sub>136</sub> [52]. Those authors also predicted the off-center displacement becomes less pronounced as x increases, in agreement with experiment [26].

Figure 5 shows the conventional cubic unit-cell volume of Na<sub>24</sub>Si<sub>136</sub> as a function of temperature for 10 K  $\leq$  *T* < 300 K, as determined from single-crystal XRD. Data for Na<sub>24</sub>Si<sub>136</sub> from 300 K < *T* < 700 K are also included, obtained from Ref. [65]. For reference, low-temperature data for Si<sub>136</sub> from Ref. [66] are shown in the inset. The thermal expansion behavior of Si<sub>136</sub> is qualitatively similar to  $\alpha$ -Si:

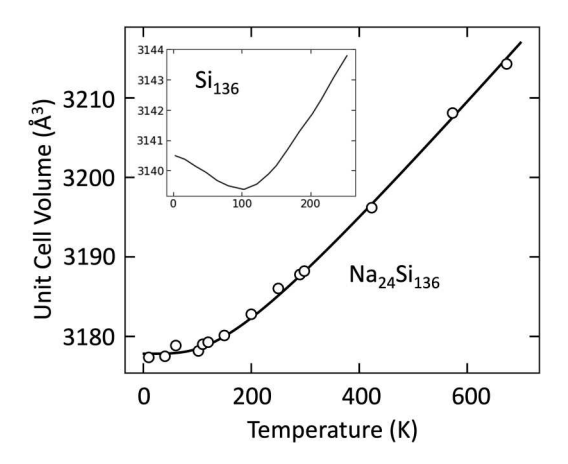


FIG. 5. Conventional unit-cell volume for  $Na_{24}Si_{136}$  as a function of temperature (data above 300 K were taken from Ref. [65]). The open circles are the experimental data, the solid curve is calculated from the Debye-Grüneisen model. The inset: Unit-cell volume vs temperature for  $Si_{136}$  (same units and scale as the main figure) from Ref. [66].

both exhibit comparable relatively small linear coefficients of thermal expansion near  $2.5 \times 10^{-6}$  K<sup>-1</sup> at room temperature and negative thermal expansion below 150 K [66,67]. In their first-principles calculations, Tang et al. [66] found a large fraction of the transverse acoustic modes have negative Grüneisen parameters in both  $\alpha$ -Si and Si<sub>136</sub> to which the negative thermal expansion can be attributed in both modifications of silicon. In contrast, the room-temperature linear coefficient of thermal expansion (CTE) of Na<sub>24</sub>Si<sub>136</sub> estimated from the data in Fig. 5 is  $7.3 \times 10^{-6} \text{ K}^{-1}$ , nearly a factor of 3 larger than for Si<sub>136</sub>. This value for the CTE of Na<sub>24</sub>Si<sub>136</sub> is in good agreement with the trend recently reported for Na<sub>x</sub>Si<sub>136</sub> (0 < x < 24) [22] as well as that for Rb<sub>12.9</sub>Si<sub>136</sub> [68]. Also, in contrast to Si<sub>136</sub>, negative thermal expansion is not observed in  $Na_{24}Si_{136}$  over the entire temperature range. Indeed, the V(T)data for Na<sub>24</sub>Si<sub>136</sub> can be well described by a conventional Debye-Grüneisen model [69],

$$V(T) = V_0 + \gamma U_D(T)/B_0,$$
 (2)

where  $V_0$  is the unit-cell volume at T = 0 K,  $\gamma$  is the mode averaged Grüneisen parameter,  $B_0$  is the bulk modulus, and the Debye vibrational energy is

$$U_D(T) = 9N_D k_B T \left(\frac{T}{\Theta_D}\right)^3 \int_0^{\Theta_D/T} \frac{x^3}{e^x - 1} dx.$$
 (3)

Here,  $N_D$  is the number of atoms per conventional unit cell,  $k_B$  is Boltzmann's constant,  $\Theta_D$  is the Debye temperature,  $x = \hbar \omega / k_B T$ ,  $\hbar$  is the reduced Planck constant, and  $\omega$  is the phonon frequency. The solid curve in Fig. 5 was calculated using  $N_D = 160$  (total number of Si and Na atoms per unit cell of Na<sub>24</sub>Si<sub>136</sub>),  $V_0 = 3178 \, \text{Å}^3$ ,  $\Theta_D = 593 \, \text{K}$  [19],  $B_0 = 85 \, \text{GPa}$  as determined from our high-pressure XRD experiments, and  $\gamma = 1.0$ . We note that  $\gamma$  and  $V_0$  are the only adjustable parameters in the model; values for all other parameters are taken from other independent experiments. The agreement between the model and the data are quite good. It is worth noting that the fit is not unique—the data could also be modeled equally

well using a combination of Debye and Einstein contributions to the vibrational energy in Eq. (2), but this adds additional parameters and complexity to the model without any significant improvement in the agreement with the experimental data. The value of  $\gamma$  for Na<sub>24</sub>Si<sub>136</sub> is more than twice that of Si<sub>136</sub> (estimated from the experimental XRD data in the positive CTE region [66]) and is consistent with the trend in values of  $\gamma$  recently reported for Na<sub>x</sub>Si<sub>136</sub> (0 < x < 24) [22] when extrapolated to x = 24. The marked increase in the obtained mode-averaged Grüneisen parameter, induced by the filling of the silicon framework cages with Na, could be due to a change in bonding related to guest-framework charge transfer, increased positive anharmonicity of the interatomic interactions, a decrease in the fraction of acoustic modes having negative mode Grüneisen parameters and/or the size of their negative mode Grüneisen parameters, or possibly some combination of these effects. The latter mechanism would also be consistent with the absence of negative thermal expansion (NTE) at low T in Na<sub>24</sub>Si<sub>136</sub>. Our first-principles calculation of the cell volume as a function of temperature in the quasiharmonic approximation captures some of the increase in positive thermal expansion in Na<sub>24</sub>Si<sub>136</sub> at high temperature (linear CTE near 300 K of approximately 4.0 K<sup>-1</sup> predicted for Na<sub>24</sub>Si<sub>136</sub> vs 2.2 K<sup>-1</sup> predicted for Si<sub>136</sub> [53]), although the magnitude of the predicted increase is somewhat smaller than observed in our experiment. Furthermore, the quasiharmonic calculation is unable to correctly predict the lack of NTE in Na<sub>24</sub>Si<sub>136</sub> at low T (see the Supplemental Material [32]). In fact, the quasiharmonic calculation predicts a more negative CTE for Na<sub>24</sub>Si<sub>136</sub> in comparison to Si<sub>136</sub>. This further suggests that our structural model and/or the quasiharmonic approximation is insufficient to capture the underlying physics of the thermal expansion in Na<sub>24</sub>Si<sub>136</sub>.

To evaluate potential differences in the chemical bonding in the silicon framework between Si<sub>136</sub> and Na<sub>24</sub>Si<sub>136</sub>, we analyzed Mulliken bond overlap populations. In this analysis, larger bond overlap population between two Si atoms suggests a stronger covalent bond. As a point of reference, the overlap population of the Si-Si bond in  $\alpha$ -Si is  $0.37e^-$  at the DFT-PBE0/TZVP level of theory. In Si<sub>136</sub>, we find the overlap populations of Si-Si bonds vary from 0.34 to 0.36e<sup>-</sup>, with an average of  $0.36e^-$ . In Na<sub>24</sub>Si<sub>136</sub>, the overlap populations vary from 0.34 to  $0.37e^-$  with an average of  $0.36e^-$ . Bond overlap populations, therefore, do not show any significant difference between Si<sub>136</sub> and Na<sub>24</sub>Si<sub>136</sub>. This analysis suggests the larger positive CTE of Na<sub>24</sub>Si<sub>136</sub> cannot be straightforwardly explained by differences in the chemical bonding within the silicon framework induced by charge transfer from the Na guest atoms.

Differences in local bonding environments, and, therefore, dynamical behavior for the Si framework atoms and the Na@Si<sub>20</sub> and Na@Si<sub>28</sub> guest atoms also manifests in the temperature dependence of the atomic displacement parameters extracted from the single-crystal diffraction refinements. Figure 6 shows the atomic displacement parameters for the silicon framework atoms (ADPs, which are  $U_{\rm eq}$  in this case; please see Ref. [32] for structure refinement details), Na@Si<sub>20</sub> guest atom, and Na@Si<sub>28</sub> guest atom as a function of temperature. The plotted ADPs in Fig. 6(b) for the silicon framework are expressed as a weighted average over the three distinct

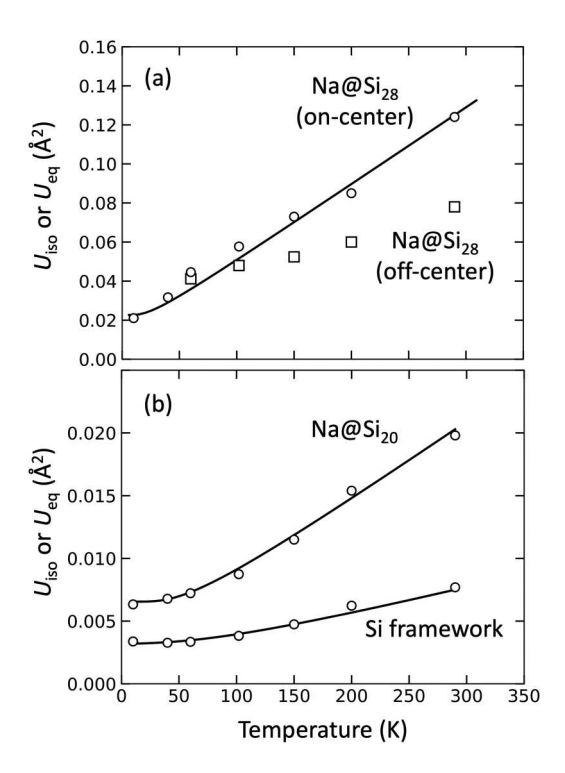


FIG. 6. Atomic displacement parameters for (a)  $Na@Si_{28}$  and (b)  $Na@Si_{20}$  and Si framework atoms, obtained from single-crystal XRD refinements. The solid curves were calculated using the models discussed in the main text.

framework crystallographic sites in the crystal structure. The silicon framework atoms show relatively small ADPs with relatively weak temperature dependence, consistent with strong covalent Si-Si bonds, whereas the Na guest ADPs are much larger and exhibit much more pronounced temperature dependence. When the Na@Si<sub>28</sub> guest atom crystallographic site is assumed to be at the center of the Si<sub>28</sub> cage (8b site), the refined ADP is enormous as has also been observed previously [26,47]. The ADP is significantly reduced in the off-center model [open squares in Fig. 6(a)] but remains quite large. As noted above, the refined Na@Si<sub>28</sub> displacement essentially becomes zero below 50 K, thus, only the on-center model was used below this temperature.

The ADPs for the Si framework atoms can be well described using a (harmonic) Debye model where the isotropic atomic displacement parameter  $U_{iso}$  is given by [70,71]

$$U_{\rm iso}(T) = \frac{3\hbar^2 T}{mk_{\rm B}\Theta_{\rm D}^2} \left(\frac{T}{\Theta_{\rm D}} \int_0^{\Theta_{\rm D}/T} \frac{x}{e^x - 1} dx + \frac{\Theta_{\rm D}}{4T}\right) + d^2,\tag{4}$$

where m is the atomic mass and  $d^2$  is a static (temperature-independent) displacement due to disorder [66]. On the other hand, the ADPs for the Na guest atoms can be described with an (also harmonic) Einstein model, where  $U_{\rm iso}$  is given by [71,72]

$$U_{\rm iso}(T) = \frac{h^2}{2mk_{\rm B}\Theta_{\rm E}} \coth\frac{\Theta_{\rm E}}{2T} + d^2, \tag{5}$$

where  $\Theta_E$  is the characteristic Einstein temperature. The solid curves in Fig. 6 were calculated using these equations and

TABLE II. Parameters used in modeling the atomic displacement parameters by Eq. (4) (Si framework) and Eq. (5) (Na guests).

Atom	$\Theta_{E}(K)$	$\Theta_{\mathrm{D}}\left(\mathrm{K}\right)$	d (Å)
Si framework	N/A	480	0.024
Na@Si <sub>20</sub>	160	N/A	0.039
Na@Si <sub>28</sub>	64	N/A	0.100

the parameters reported in Table II. The d values for the Si framework and the Na@Si20 guest are both relatively small and comparable to those reported for type-I clathrates [1,64]. The Einstein temperature for Na@Si<sub>20</sub> (160 K) is in very good agreement with the value obtained by fits to heat-capacity data (166 K) [19] as well as the phonon frequencies from our first-principles calculations above. We again note that our first-principles calculation of the phonon dispersion (Fig. 2) indicates that the Na@Si20 guest vibrations have a range of frequencies as opposed to the simplified assumption of a single Einstein frequency, but the simplified Einstein model is, nevertheless, sufficient to capture the behavior of the ADPs. In contrast, the Debye temperature for the Si framework atoms (480 K) is substantially lower than that obtained from heatcapacity measurements (593 K). Interestingly, the Einstein temperature for the Na@Si28 guest (64 K) when Na is assumed on-center, is in relatively good agreement with that obtained from heat-capacity modeling (55 K) [19] and the corresponding energy is comparable to that obtained from powder INS [47], whereas the value of d is quite large. In contrast, the Einstein temperature implied by the ADPs in the off-center model is significantly higher, inconsistent with INS as well as our first-principles calculations above. These results provide further indication that the positional and dynamical behavior of the Na@Si<sub>28</sub> guest is complex and not captured by the simpler models applied here.

# V. CONCLUSION

High-pressure XRD measurements show that the Na guest atoms effect a pronounced enhancement of the pressure stability of Na<sub>24</sub>Si<sub>136</sub> relative to guest-free Si<sub>136</sub>, suggesting the guest atoms inhibit the pathway for volume collapse of the clathrate framework. Despite chemical pressure effects that might be expected to increase the bulk modulus upon filling the voids of the Si<sub>136</sub> framework with Na, the bulk modulus of Na<sub>24</sub>Si<sub>136</sub> is slightly smaller than that of guest-free Si<sub>136</sub>. In contrast to Si<sub>136</sub>, no negative thermal expansion is observed in Na<sub>24</sub>Si<sub>136</sub> for which the thermal expansion is described relatively well by the conventional Debye-Grüneisen model.

Whereas the Na@Si<sub>28</sub> guest must be assumed to be off-center to produce sensible results in calculations of phonon dispersion, the exact nature of the off-centering and dynamical behavior of the guest have yet to be determined unequivocally. In particular, from temperature-dependent single-crystal synchrotron XRD, the refined displacement of Na@Si<sub>28</sub> in an off-center model reduces to zero as the temperature is decreased with essentially no difference between on-center and off-center models below 50 K, whereas first-principles calculation suggests the presence of multiple off-center equilibrium positions. Low-energy modes associated with the Na guest atoms are clearly observed in the first-principles phonon dispersion and vibrational density of states, confirming the origin of qualitative features observed in previous experimental inelastic neutron-scattering and heat-capacity measurements. Temperature-dependent single-crystal neutron diffraction as well as pressure- and temperature-dependent inelastic neutron-scattering experiments from Na<sub>24</sub>Si<sub>136</sub> would likely yield important insights into the nature of the Na@Si<sub>28</sub> guest as well as anharmonicity. Although specimens of sufficient size for such experiments are not yet readily available, continuing advances in the growth of single crystals of Na-Si clathrates [40,48,73] may make this a possibility in the future.

## ACKNOWLEDGMENTS

A.J.K. thanks the Academy of Finland for funding (Grant Nno. 317273) and CSC-The Finnish IT Center for Science for computational resources. A.Z. and W.P. acknowledge support from DOE-BES Grant No. DE-SC0019252 for high-pressure structure investigations. G.S.N. acknowledges support by National Science Foundation Grant No. DMR-1748188. C.P., A.J., and E.C. were Frost Summer and/or Academic Year Research Scholars at Cal Poly and thank the William and Linda Frost Fund for support. Portions of this work were performed at HPCAT (Sector 16), APS, Argonne National Laboratory. HPCAT operations are supported by DOE-NNSA's Office of Experimental Sciences. We gratefully acknowledge ChemMatCARS Sector 15 which is principally supported by the National Science Foundation/Department of Energy under Grant No. NSF/CHE-1834750. The Advanced Photon Source is a U.S. Department of Energy (DOE) Office of Science User Facility operated for the DOE Office of Science by Argonne National Laboratory under Contract No. DE-AC02-06CH11357. Crystal structure representations were created with the VESTA software [74]. Interatomic distance calculations were performed using the GSAS-II software package [75].

<sup>[1]</sup> *The Physics and Chemistry of Inorganic Clathrates*, edited by G. S. Nolas (Springer, Dordrecht, 2014).

<sup>[2]</sup> J. Gryko, P. F. McMillan, R. F. Marzke, G. K. Ramachandran, D. Patton, S. K. Deb, and O. F. Sankey, Phys. Rev. B 62, R7707(R) (2000).

<sup>[3]</sup> A. M. Guloy, R. Ramlau, Z. Tang, W. Schnelle, M. Baitinger, and Y. Grin, Nature (London) 443, 320 (2006).

<sup>[4]</sup> M. Beekman, K. Wei, and G. S. Nolas, Appl. Phys. Rev. 3, 040804 (2016).

<sup>[5]</sup> M. Beekman and G. S. Nolas, Physica B 383, 111 (2006).

<sup>[6]</sup> A. San-Miguel, P. Kéghélian, X. Blase, P. Mélinon, A. Perez, J. P. Itié, A. Polian, E. Reny, C. Cros, and M. Pouchard, Phys. Rev. Lett. 83, 5290 (1999).

<sup>[7]</sup> G. K. Ramachandran, P. F. McMillan, S. K. Deb, M. Somayazulu, J. Gryko, J. Dong, and O. F. Sankey, J. Phys.: Condens. Mater. 12, 4013 (2000).

<sup>[8]</sup> G. S. Nolas, J. L. Cohn, G. A. Slack, and S. B. Schujman, Appl. Phys. Lett. 73, 178 (1998).

- [9] J. Dolyniuk, B. Owens-Baird, J. Wang, J. V. Zaikina, and K. Kovnir, Mater. Sci. Eng. R: Rep. 108, 1 (2016).
- [10] J. L. Cohn, G. S. Nolas, V. Fessatidis, T. H. Metcalf, and G. A. Slack, Phys. Rev. Lett. 82, 779 (1999).
- [11] T. Takabatake, K. Suekuni, T. Nakayama, and E. Kaneshita, Rev. Mod. Phys. 86, 669 (2014).
- [12] M. Christensen, A. B. Abrahamsen, N. B. Christensen, F. Juranyi, N. H. Andersen, K. Lefmann, J. Andreasson, C. R. H. Bahl, and B. B. Iversen, Nature Mater. 7, 811 (2008).
- [13] J. Dong, O. F. Sankey, and C. W. Myles, Phys. Rev. Lett. 86, 2361 (2001).
- [14] M. Beekman and A. VanderGraaff, J. Appl. Phys. 121, 205105 (2017).
- [15] A. Prokofiev, A. Sidorenko, K. Hradil, M. Ikeda, R. Svagera, M. Waas, H. Winkler, K. Neumaier, and S. Paschen, Nature Mater. 12, 1096 (2013).
- [16] M. Beekman and G. S. Nolas, J. Mater. Chem. 18, 842 (2008).
- [17] J. S. Kasper, P. Hagenmuller, M. Pouchard, and C. Cros, Science 150, 1713 (1965).
- [18] C. Cros, M. Pouchard, and P. Hagenmuller, J. Solid State Chem. 2, 570 (1970).
- [19] M. Beekman, W. Schnelle, H. Borrmann, M. Baitinger, Yu. Grin, and G. S. Nolas, Phys. Rev. Lett. 104, 018301 (2010).
- [20] S. Stefanoski, C. D. Malliakas, M. G. Kanatzidis, and G. S. Nolas, Inorg. Chem. **51**, 8686 (2012).
- [21] A. D. Ritchie, M. B. Johnson, J. F. Niven, M. Beekman, G. S. Nolas, J. Gryko, and M. A. White, J. Phys.: Condens. Matter 25, 435410 (2013).
- [22] M. Beekman, J. A. Kaduk, W. Wong-Ng, M. Troesch, G. S. Lee, and G. S. Nolas, Appl. Phys. Lett. 112, 181901 (2018).
- [23] G. S. Nolas, M. Beekman, J. Gryko, G. A. Lamberton, Jr., T. M. Tritt, and P. F. McMillan, Appl. Phys. Lett. 82, 910 (2003).
- [24] V. J. Härkönen and A. J. Karttunen, Phys. Rev. B 93, 024307 (2016).
- [25] G. B. Adams, M. O'Keeffe, A. A. Demkov, O. F. Sankey, and Y.-M. Huang, Phys. Rev. B 49, 8048 (1994).
- [26] M. Beekman, E. N. Nenghabi, K. Biswas, C. W. Myles, M. Baitinger, Y. Grin, and G. S. Nolas, Inorg. Chem. 49, 5338 (2010).
- [27] J. P. Perdew, K. Burke, and M. Ernzerhof, Phys. Rev. Lett. 77, 3865 (1996).
- [28] K. F. Garrity, J. W. Bennett, K. M. Rabe, and D. Vanderbilt, Comput. Mater. Sci. 81, 446 (2014).
- [29] P. Giannozzi, O. Andreussi, T. Brumme, O. Bunau, M. Buongiorno Nardelli, M. Calandra, R. Car, C. Cavazzoni, D. Ceresoli, M. Cococcioni *et al.*, J. Phys.: Condens. Matter 29, 465901 (2017).
- [30] A. Togo and I. Tanaka, Scripta Mater. 108, 1 (2015).
- [31] A. Togo, L. Chaput, I. Tanaka, and G. Hug, Phys. Rev. B **81**, 174301 (2010).
- [32] See Supplemental Material at http://link.aps.org/supplemental/ 10.1103/PhysRevB.105.214114 for crystallographic data from single-crystal x-ray diffraction (XRD) refinements, structure model for phonon dispersion calculations, theoretically calculated Na@Si<sub>28</sub> guest displacement as a function of pressure, and calculated CTE vs temperature in the quasiharmonic approximation.
- [33] A. Dal Corso, thermo\_pw, a driver of quantum-ESPRESSO routines for the automatic computation of ab-initio material properties, https://dalcorso.github.io/thermo\_pw/

- [34] R. Dovesi, A. Erba, R. Orlando, C. M. Zicovich-Wilson, B. Civalleri, L. Maschio, M. Rérat, S. Casassa, J. Baima, S. Salustro, and B. Kirtman, Wiley Interdiscip. Rev.: Comput. Mol. Sci. 8, 1 (2018).
- [35] C. Adamo and V. Barone, J. Chem. Phys. 110, 6158 (1999).
- [36] F. Weigend and R. Ahlrichs, Phys. Chem. Chem. Phys. 7, 3297 (2005).
- [37] A. J. Karttunen, T. F. Fässler, M. Linnolahti, and T. A. Pakkanen, Inorg. Chem. 50, 1733 (2011).
- [38] R. E. Stene, B. Scheibe, A. J. Karttunen, W. Petry, and F. Kraus, Eur. J. Inorg. Chem. 2019, 3672 (2019).
- [39] A. Erba, A. Mahmoud, D. Belmonte, and R. Dovesi, J. Chem. Phys. 140, 124703 (2014).
- [40] S. Stefanoski, M. Beekman, W. Wong-Ng, P. Zavalij, and G. S. Nolas, Chem. Mater. 23, 1491 (2011).
- [41] G. Shen, Y. Wang, A. Dewaele, C. Wu, D. E. Fratanduono, J. Eggert, S. Klotz, K. F. Dziubek, P. Loubeyre, O. V. Fat'yanov et al., High Pressure Res. 40, 299 (2020).
- [42] C. Prescher and V. B. Prakapenka, High Pressure Res. 35, 223 (2015).
- [43] M. Wojdyr, J. Appl. Crystallogr. 43, 1126 (2010).
- [44] APEX3. Program for Bruker CCD X-ray Diffractometer Control (Bruker AXS, Madison, WI, 2009).
- [45] G. M. Sheldrick, *SHELXTL*, version 2018/3. Program for Solution and Refinement of Crystal Structures (Universität Göttingen, Göttingen, Germany).
- [46] G. M. Sheldrick, Acta Cryst. C71, 3 (2015).
- [47] M. Beekman, R. P. Hermann, A. Möchel, F. Juranyi, and G. S. Nolas, *J. Phys.: Condens. Matter* **22**, 355401 (2010).
- [48] M. Beekman, M. Baitinger, H. Borrmann, W. Schnelle, K. Meier, G. S. Nolas, and Yu. Grin, J. Am. Chem. Soc. 131, 9642 (2009).
- [49] F. Brunet, P. Mélinon, A. San Miguel, P. Kéghélian, A. Perez, A. M. Flank, E. Reny, C. Cros, and M. Pouchard, Phys. Rev. B 61, 16550 (2000).
- [50] F. Tournus, B. Masenelli, P. Mélinon, D. Connétable, X. Blase, A. M. Flank, P. Lagarde, C. Cros, and M. Pouchard, Phys. Rev. B 69, 035208 (2004).
- [51] T. Ban, T. Ogura, Y. Ohashi, R. Himeno, F. Ohashi, T. Kume, Y. Ohya, H. Natsuhara, T. Iida, H. Habuchi, and S. Nonomura, J. Mater. Sci. 48, 989 (2013).
- [52] D. Xue and C. W. Myles, Materials 12, 536 (2019).
- [53] V. J. Härkönen and A. J. Karttunen, Phys. Rev. B 89, 024305 (2014).
- [54] J. S. Tse, V. P. Shpakov, V. V. Murashov, and V. R. Belosludov, J. Chem. Phys. 107, 9271 (1997).
- [55] P. Mélinon, P. Kéghélian, A. Perez, B. Champagnon, Y. Guyot, L. Saviot, E. Reny, C. Cros, M. Pouchard, and A. J. Dianoux, Phys. Rev. B 59, 10099 (1999).
- [56] W. Setyawan and S. Curtarolo, Comput. Mater. Sci. 49, 299 (2010).
- [57] A. San-Miguel and P. Toulemonde, High Pressure Res. 25, 159 (2005).
- [58] F. P. Bundy and J. S. Kasper, High Temp.-High Pressures 2, 429 (1970).
- [59] F. J. Birch, J. Geophys. Res.: Space Phys. 83, 1257 (1978).
- [60] F. D. Murnaghan, Proc. Natl. Acad. Sci. USA 30, 244 (1944).
- [61] J. E. F. S. Rodrigues, J. Gainza, F. Serrano-Sánchez, M. M. Ferrer, G. S. L. Fabris, J. R. Sambrano, N. M. Nemes, J. L.

- Martínez, C. Popescu, and J. A. Alonso, Inorg. Chem. **60**, 7413 (2021).
- [62] N. Ishimatsu, K. Yokoyama, T. Onimaru, T. Takabatake, K. Suekuni, N. Kawamura, S. Tsutsui, M. Mizumaki, T. Ina, T. Watanuki et al., J. Phys. Soc. Jpn. 88, 114601 (2019).
- [63] T. Sukemura, T. Kume, T. Matsuoka, S. Sasaki, T. Onimaru, and T. Takabatake, J. Phys.: Conf. Ser. 500, 182022 (2014).
- [64] M. Christensen, N. Lock, J. Overgaard, and B. B. Iversen, J. Am. Chem. Soc. 128, 15657 (2006).
- [65] I. Veremchuk, L. Vasylechko, B. Böhme, M. Baitinger, D. Trots, and Y. Grin, Photon Science (2009). Highlights and HA-SYLAB Annual Report (Deutsches Elektronen-Synchrotron, a research centre of the helmholtz assoc.), Hamburg, 2009, p. 752 (unpublished).
- [66] X. Tang, J. Dong, P. Hutchins, O. Shebanova, J. Gryko, P. Barnes, J. K. Cockcroft, M. Vickers, and P. F. McMillan, Phys. Rev. B 74, 014109 (2006).

- [67] J. S. Shah and M. E. Straumanis, Solid State Commun. 10, 159 (1972).
- [68] W. D. C. B. Gunatilleke, O. P. Ojo, H. Poddig, and G. S. Nolas, J. Solid State Chem. 311, 123152 (2022).
- [69] E. Grüneisen, Handb. Phys. 10, 1 (1926).
- [70] K. Lonsdale, Acta Crystallogr. 1, 142 (1948).
- [71] B. T. M. Willis and A. W. Pryor, *Thermal Vibrations in Crystallography* (Cambridge University Press, London, 1975).
- [72] J. D. Dunitz, V. Schomaker, and K. N. Trueblood, J. Phys. Chem. 92, 856 (1988).
- [73] H. Morito, H. Yamane, R. Y. Umetsu, and K. Fujiwara, Crystals 11, 808 (2021).
- [74] K. Momma and F. Izumi, J. Appl. Crystallogr. 44, 1272 (2011).
- [75] B. H. Toby and R. B. Von Dreele, J. Appl. Crystallogr. 46, 544 (2013).